TABLE 1. FIT OF SELF-DIFFUSION DATA FOR n-HEXANE TO EQ. 1

T/K	a^1	b^1	σ^2	Range[3]
223.15	0.4622	−0.0308	2.0	48.7-292.3
248.15	0.8968	−0.0273	1.9	55.7-391.2
273.15	1.1763	−0.0241	0.4	25.0-393.8
298.15	1.4513	−0.0221	0.9	0.1-353.5
333.15	1.7746	−0.0206	0.9	0.1-392.4

[1] Values obtained by expressing $ln\ (10^9 D/m^2 \cdot s^{-1})$ as a linear function of (P/MPa).
[2] Mean deviation (%) of experimental points from values calculated from equations to the lines of best fit.
[3] Lowest experimental pressure (MPa) for which D is predicted within experimental uncertainty by Eq. 1, and highest experimental pressure.

temperatures are plotted in Figure 1. The variation of D with P for n-hexane is typical normal liquid behavior. The slopes of the curves decrease considerably with increasing pressure, particularly at elevated temperatures. Clearly the pressure dependence of D is so strong that if data were available up to only 200 MPa, for example, it would be difficult to reliably extrapolate the curves to much higher pressures. The data at each temperature could no doubt be fitted to functions such as polynomials in P for extrapolation purposes, but (depending on the order of the polynomial) a considerable number of data points may be required, so that polynomials have limited value as predictive functions. Fits of the n-hexane data to Eq. 1 are shown in Figure 2, which demonstrates that apart from the low pressure (<50 MPa) region at low temperatures, the plots are linear up to the highest pressures attained in the measurements. The best-fit parameters of Eq. 1 are listed in Table 1. The estimated accuracy of the experimental data is ±2.5%, so that for each temperature the mean deviation is smaller than the uncertainty in individual data points. Since Eq. 1 has only two adjustable parameters, as few as two experimental diffusion coefficients at pressures above say 50 MPa are adequate to make good estimates of D at other pressures.

The general applicability of Eq. 1 suggests that it can serve also as a useful criterion of normal liquid behavior. The relationship does not hold for tracer and self-diffusion coefficients of water. However, the variation of D with P for water is abnormal in that with increasing pressure D first increases, then subsequently decreases (Woolf, 1975; Woolf and Harris, 1980). Work in progress on tracer diffusion of methanol has revealed a similar anomaly at low temperature. At higher temperature the diffusion of methanol in water approaches normal liquid behavior.

NOTATION

D = self-diffusion or tracer diffusion coefficient, $m^2 \cdot s^{-1}$
P = pressure, MPa

LITERATURE CITED

Harris, K. R., "The Temperature and Density Dependence of the Self-Diffusion Coefficient of n-Hexane from 223 to 333 K and to 400 MPa," *J.C.S. Faraday I*, 78 (1982).

Harris, K. R., and L. A. Woolf, "Pressure and Temperature Dependence of the Self-Diffusion Coefficient of Water and Oxygen-18 Water," *J.C.S. Faraday I*, **76**, p. 377 (1980).

Woolf, L. A., "Tracer Diffusion of Tritiated Water (THO) in Ordinary Water (H_2O) under Pressure," *J.C.S. Faraday I*, **71**, p. 784 (1975).

Manuscript received February 11, 1982; revision received April 12, and accepted April 26, 1982.

Reconstruction of Oil Saturation Distribution Histories During Immiscible Liquid-Liquid Displacement by Computer-Assisted Tomography

S. Y. WANG, SEYDA AYRAL, F. S. CASTELLANA, and CARL C. GRYTE

Department of Chemical Engineering and Applied Chemistry
Columbia University
New York, NY 10027

INTRODUCTION

Characterization of the fluid mechanics of immiscible displacement of one liquid phase by another in porous media in connection with oil recovery processes requires knowledge of the time history of the intramedia spatial distribution of each phase. Such distributions in optically dense media are difficult to obtain because of the inaccessibility to traditional measurement probes.

Several methods have been used, however, to study flow behavior in such systems. Fluid solidification by polymerization with subsequent sectioning has detailed the final fluid distribution. Microwave attenuation (Parsons, 1975) and conductivity measurements (Leverett, 1939) give area-average fluid saturations. Measurements of the distribution of a radionuclide tracer using a

Correspondence concerning this paper should be directed to C. C. Gryte.

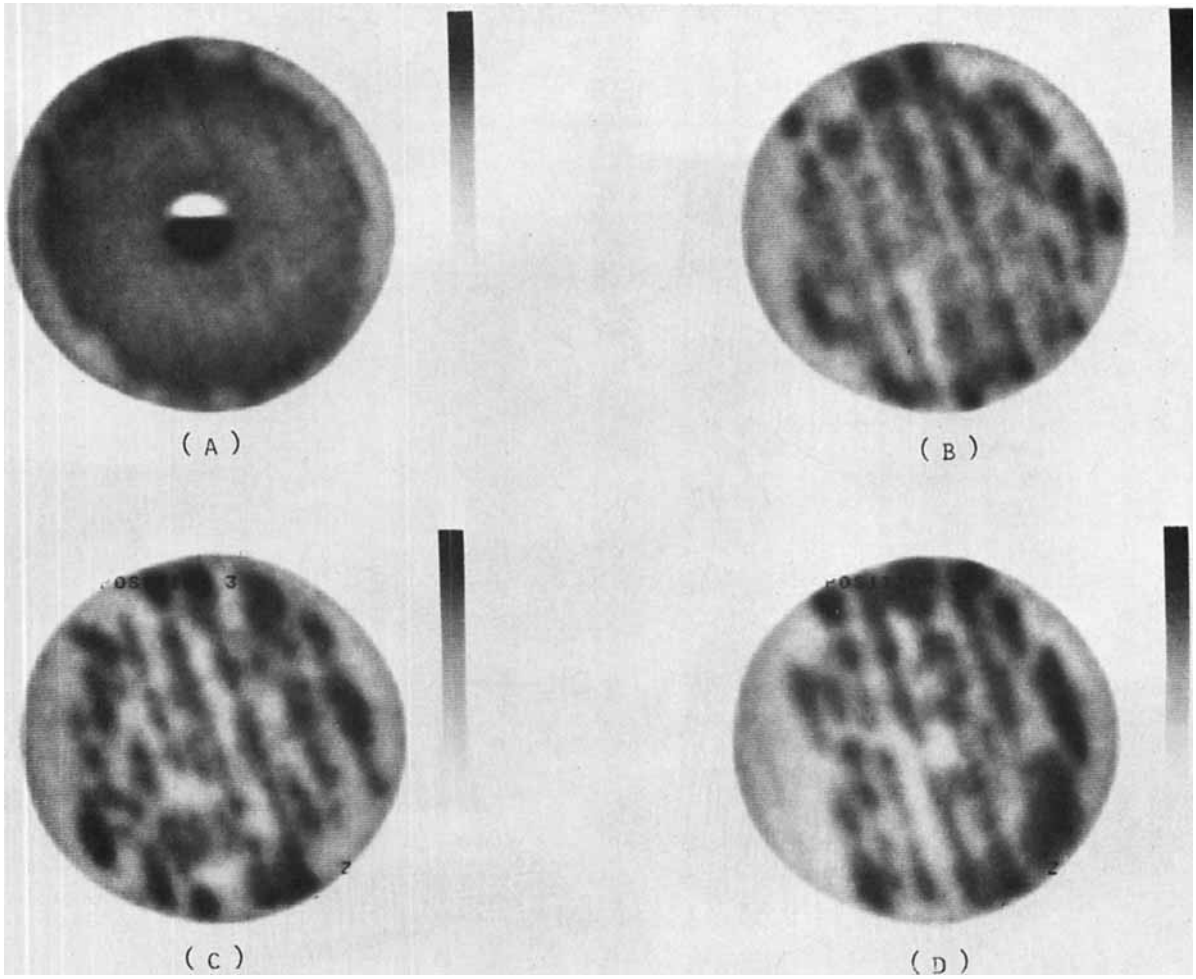

Figure 1. Gray-scale display of oil saturation distribution at four axial positions. Dark regions are water-rich and light regions are oil-rich. (a) 2.5 cm, (b) 6.0 cm, (c) 10.3 cm, and (d) 15.5 cm from the injection point.

Gamma Camera (Castellana et al., 1980) provides two-dimensional projections of the fluid distributions. Transparent porous models (van Meurs, 1957) show the motion of the fluid interface, although they do not yield quantitative data. X-ray shadowgraphs (Slobod and Caudle, 1952) give only pictorial representations of the fluid distributions. None of these methods, however, provides the detailed information required for a conclusive study of the two-phase immiscible displacement process.

EXPERIMENTAL

In the present study, we demonstrate that computer-assisted tomography (Ambrose, 1973) can provide fluid saturation data as a function of spatial position and time during dynamic oil displacement experiments. An unmodified second generation CAT scanner (DeltaScan-50 CT Scanner, Technicare, Inc.) was used to obtain oil distribution histories. The porous media models used in this laboratory are cylindrical Berea sandstone cores (5 cm in diameter and 25 cm in length) obtained from Cleveland Quarries. The permeability of the core is 300 millidarcies. The core was initially evacuated and then filled completely with oil (Texaco, 70 pale crude, 15 centipoise). A displacing fluid of 1 M potassium iodide was injected into the core at a rate of 10 cm^3/h (the superficial velocity is approximately 60 cm/d. This concentration of electrolyte was selected because its X-ray attenuation was demonstrated in preliminary calibration tests to provide an appropriate contrast to that of the oil. At selected times following introduction of the displacing fluid, the core was placed in the CAT scanner and cross-sectional scans were made at four different axial locations (2.5, 6.0, 10.3 and 15.5 cm from the injection point). The computer unit generates two images for each scan, displaced in distance by 0.5 cm. The image data are composed of local X-ray attenuation coefficients within the scanned cross-section for pixel elements $0.8 \times 0.8\ mm^2 \times .8$ cm deep. The amount of oil and water recovered was recorded as a function of time. The experiments were stopped after collection of 3 pore volumes (one pore volume is about 108 mL), when practically no more oil was seen to be removed from the sandstone formation.

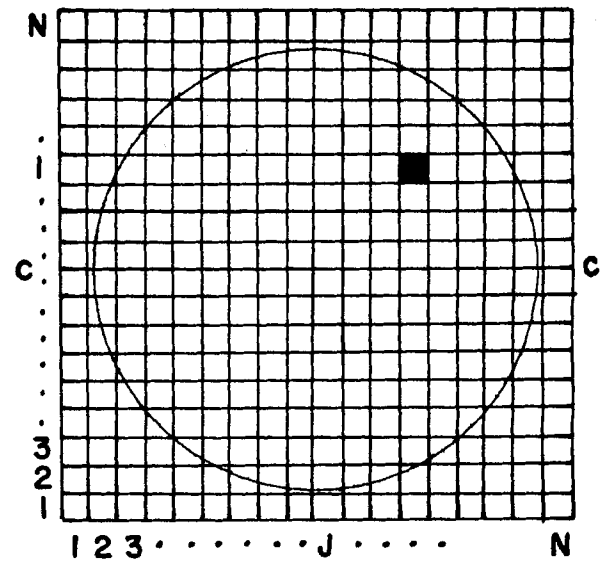

Figure 2. Schematic diagram showing volume element (*I*,*J*) and central traverse C-C.

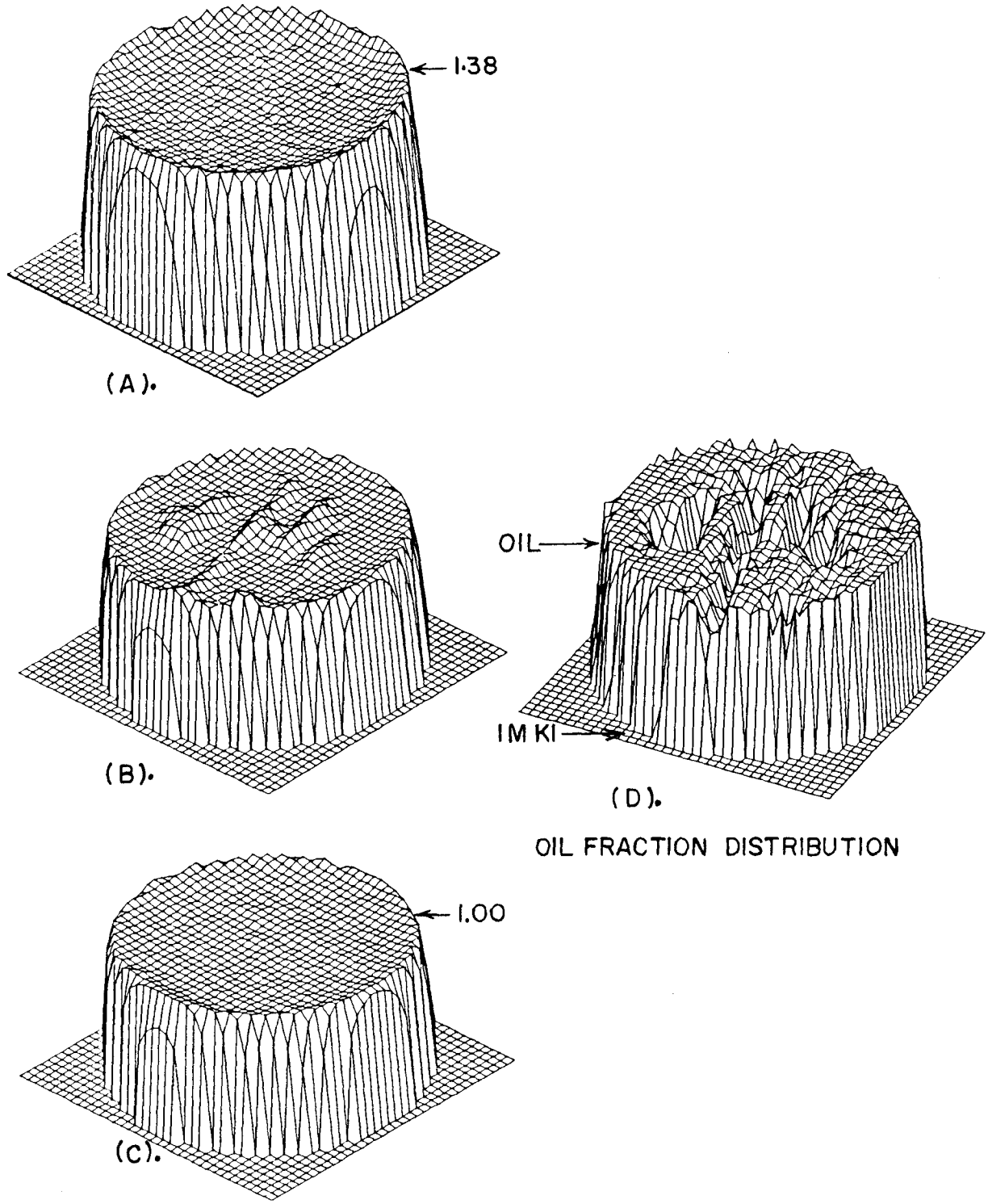

Figure 3. Oil fraction distribution. Oil fraction distribution computed from X-ray attenuation coefficient distributions obtained from CAT scanner. (a) X-ray attenuation coefficient of 1 M KI core. (b) X-ray attenuation coefficient of 1 M KI/oil mixture core. (c) X-ray attenuation coefficient of oil core. (d) Oil fraction distribution of 1 M KI/oil mixture core. (Condition: 7.6 cm from the injection point; 4.5% pore volume of 1 M KI injected.)

RECONSTRUCTION OF OIL SATURATION DISTRIBUTION HISTORIES

The local X-ray attenuation coefficient of each volume element (pixel) is related to its composition, i.e., the relative amount of sandstone formation and the fluid mixture occupying the void spaces. From these linear attenuation coefficients the fluid saturation in the pore space of each volume element can be evaluated. Figures 1(a)–(d) show gray-scale display of the scanned images taken at four axial positions after injecting a volume of KI solution equal to 3 pore volumes. The darker regions indicate water-rich areas where most of the oil has been displaced, and the lighter regions indicate oil-rich area bypassed by the displacing fluid. The regular distribution of dark and light regions suggests the presence of macroscopic regions of different permeability, i.e., the bedding planes.

The image reconstruction is based on multiple transmission X-ray measurements around the object's periphery. The attenuation coefficients (μ_{ij}) are computed using a standard reconstruction algorithm (Brooks and DiChiro, 1975). The X-ray attenuation

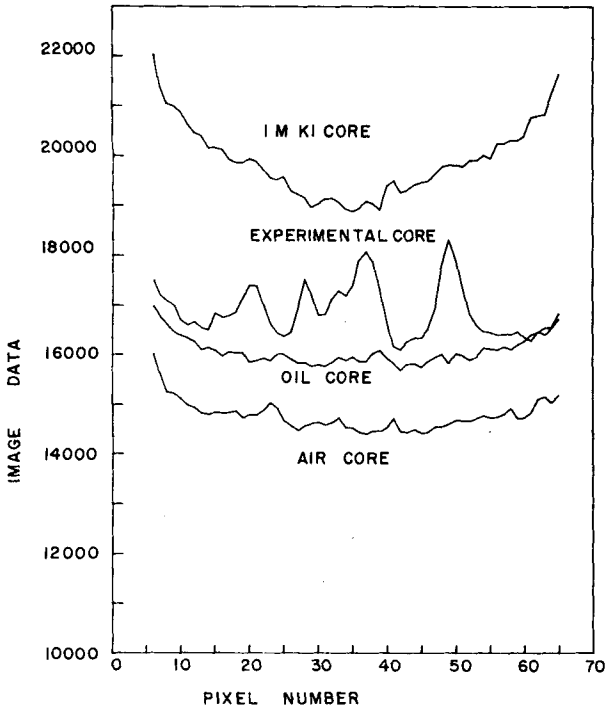

Figure 4a. Central transverses of X-ray attenuation coefficient image data.

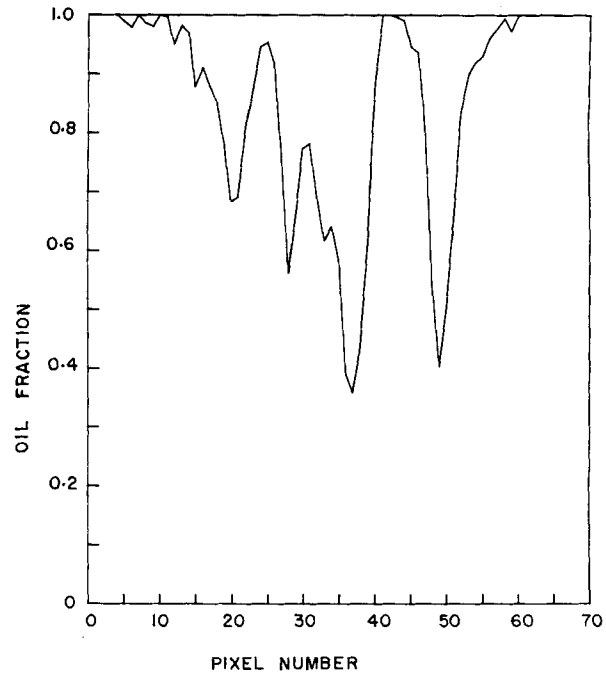

Figure 4b. Central traverse of oil fraction distribution data.

coefficient of pixel element (i,j) (Figure 2) is the linear combination of that of the solid sand and the fluid mixture (oil and 1 M KI solution).

$$\mu_{ij} = (1 - \phi_{ij})\mu_{\text{solid}} + \phi_{ij}[(1 - x_{ij})\mu_{1\text{ M KI}} + x_{ij}\mu_{\text{oil}} \quad (1)$$

where ϕ_{ij} and x_{ij} are, respectively, the void fraction and the oil fraction in the fluid mixture at pixel (i,j). $\mu_{1\text{ M KI}}$ and μ_{oil} are the attenuation coefficients of pure 1 M KI solution and oil, respectively.

If two reference cores are scanned, one filled with 1 M KI solution and the other filled with oil, the X-ray attenuation coefficients at pixel (i,j) for these cores are given by

$$\mu^{ij}_{\text{oil core}} = (1 - \phi_{ij})\mu_{\text{solid}} + \phi_{ij}\mu_{\text{oil}} \quad (2)$$

$$\mu^{ij}_{\text{1 M KI core}} = (1 - \phi_{ij})\mu_{\text{solid}} + \phi_{ij}\mu_{1\text{ M KI}} \quad (3)$$

Combining Eqs. 1, 2 and 3 yields an expression for the local oil fraction.

$$x_{ij} = \frac{\mu_{ij} - \mu^{ij}_{\text{1 M KI core}}}{\mu^{ij}_{\text{oil core}} - \mu^{ij}_{\text{1 M KI core}}} \quad (4)$$

The image data are stored on magnetic tape as numbers proportional to the local X-ray attenuation coefficients. These data for the experimental core and the two reference cores may be substituted into Eq. 4, and the oil saturation distribution within each scanned cross section computed. Figure 3 shows the initial image data and the computed oil fraction distribution. The substantial differences between data derived from the 1 M KI core and the oil core (Figure 4(a), (c)) indicate that the oil fractions within the fluid mixture can be calculated. The central traverses (Figure 2) of these diagrams are plotted in Figure 4, and the periodic variation in the X-ray attenuation numbers of the experimental core is seen to be consistent with the fluid distribution structure shown by the gray-scale picture, Figure 1(b). The period of the variation is about 6 to 12 image elements which indicates a macroscopic bedding plane thickness in the range of 0.5 to 1 cm. Similar spatial resolution has been reported by Genant and Boyd (1977), who used an EMI scanner (image element size, 1.5 mm) to identify 4 mm K_2HPO_4 phantoms in an aqueous environment. Also, McCullough et al. (1976) report a high-contrast resolution of 1.25 mm for the Delta 50 CT Scanner. We are thus confident that the data obtained is significant in its identification of oil-rich and water-rich domains in the sandstone core.

By making consecutive measurements at different axial positions and different times, the oil saturation distributions can be obtained as a function of spatial position and time. Average oil saturation obtained from integrating the oil distribution at each cross section in the axial direction of the core is in close agreement with that obtained from the overall mass balance and output measurement. The dynamics of the displacement process may be observed when the flow is slow relative to the scanning speed. The exact structure and motion of viscous "fingers" associated with the immiscible displacement process can be reconstructed and thus permit a more detailed analysis of fluid behavior. The time derivatives of the fluid saturations can also be computed and used in the flow equations to compute the local flow velocity. The information obtained from CAT scan experiments is very valuable in studying the stability of the fluid interface (the displacement front) during immiscible displacement.

DISCUSSION

Beam Hardening

As a result of the nonmonochromatic character of the X-ray beam, lower energy X-rays are preferentially absorbed, and beams passing through the central region of a circular cross section have relatively higher energy than those passing through the periphery. The computed X-ray attenuation coefficients of the central region are thus less than that of the outer region. This "cupping" artifact is seen in Figure 4(a). However, since the oil fractions are computed by the "differences" between CT images the beam hardening effect is minimized.

Limits of Resolution

The spatial resolution of the CAT scanner employed in this experiment is approximately 0.8 × 0.8 mm × 8 mm which is about two orders of magnitude higher than the microscopic pore sizes of ordinary reservoir rock formations. Although no direct observations of micropore flow is currently possible, the macroscopic frontal instabilities can be clearly demonstrated, and the porosity

stratifications of the sandstone structure identified. It is evident from this preliminary investigation that CAT scanning is an effective means of observing the mechanism involved in immiscible displacement processes. Further studies are being undertaken to differentiate the variables affecting the oil recovery processes.

ACKNOWLEDGMENT

We would like to acknowledge M. Hodora and J. Bond of the Department of Radiology, St. Luke's Hospital Center, for their technical assistance in operating the CAT scan facilities. We also wish to thank The National Science Foundation (CPE-81-20846).

NOTATION

x_{ij} = oil fraction (volume fraction) of fluid mixture occupying the void space at element (i,j), δ

ϕ_{ij} = volume fraction of the void space at element (i,j), δ

μ_{ij} = X-ray attenuation coefficient of volume element (i,j), cm^{-1}

$\mu_{oil,\ 1\ M\ KI}$ = X-ray attenuation coefficient of pure oil, 1 M KI solution, respectively, cm^{-1}

$\mu_{\substack{oil\ core \\ 1\ M\ KI\ core}}$ = X-ray attenuation coefficient of volume element (i,j) of the porous material when completely filled with oil, pure 1 M KI solution, respectively, cm^{-1}

Note: μ_{oil} and $\mu_{oil\ core}$ are different in that μ_{oil} is a physical property of pure oil and $\mu_{oil\ core}$ expresses the combining X-ray attenuation effect of both oil and the solid porous structure.

LITERATURE CITED

Ambrose, J., "Computerized Transverse Axial Scanning (Tomography). Part II. Clinical Application," *Brit. J. Radiol.*, **46**, 1023 (1973).

Brooks, R. A., and G. DiChiro, "Theory of Image Reconstruction in Computed Tomography," *Radiology*, **117**, 561 (1975).

Castellana, F. S., J. L. Spencer, and A. Cartolano, "Application of the Gamma Camera to Studies of Flow and Mixing in Reactor Vessels," *Ind. Eng. Chem. Fund.*, **19**, 222 (1980).

Genant, H. K., and D. Boyd, "Quantitative Bone Mineral Analysis Using Dual Energy Computed Tomography," *Invest. Radiol.*, **12**, 545 (1977).

Leverett, M. C., "Flow of Oil-Water Mixtures through Unconsolidated Sands," *Trans. AIME*, **132**, 149 (1939).

McCullough, E., et al., "Performance Evaluation and Quality Assurance of Computed Tomography Scanners with Illustrations from the EMI, ACTA and DELTA Scanners," *Radiology*, **120**, 173 (1976).

van Meurs, P., "The Use of Transparent Three-Dimensional Models for Studying the Mechanism of Flow Process in Oil Reservoirs," *Trans. AIME*, **210**, 295 (1957).

Parsons, R. W., "Microwave Attenuation—A New Tool for Monitoring Saturation in Laboratory Flooding Experiments," *Soc. Petrol. Engrs. J.*, **15**, 302 (1975).

Slobod, R. L., and B. H. Caudle, "X-Ray Shadowgraph Studies of Areal Sweepout Efficiencies," *Trans. AIME*, **195**, 265 (1952).

Manuscript received August 24, 1982; revision received January 14, and accepted January 24, 1983.

Single-Pellet Reactor for Bidisperse Porous Catalysts

DEEPAK KUNZRU

Department of Chemical Engineering
Indian Institute of Technology, Kanpur
Kanpur 208016, India

A single-pellet reactor has been shown to be an elegant method for determining the intrinsic rate constant, effective diffusivity and the effectiveness factor for monodisperse catalysts. In addition, by measuring the center plane concentration with time for a deactivating catalyst, information can be obtained on the mechanism and kinetics of the poisoning process. The experimental and analytical details of a single-pellet reactor have been discussed elsewhere (Hegedus and Peterson, 1974).

Very often the catalyst is formed by pelletizing small microspherical porous particles resulting in a bidisperse porous catalyst. Diffusion in both the macropores and the micropores affects the overall effectiveness factor. Generally, the effectiveness factor for the particles is assumed to be unity and, with this approximation, the expressions for the effectiveness factor for mono- and bidisperse catalysts become identical. However, if the reaction is fast, the effectiveness factor for the particles can be less than unity and the above approximation is no longer valid. Örs and Dõgu (1979) discussed the effectiveness factor of bidisperse catalysts and the error involved if this is approximated as monodisperse. A procedure for incorporating the pore size distribution in the macro- and micropores in calculating effectiveness factors is available (Mingle and Smith, 1961). Effectiveness factors for reversible reactions in bidisperse catalysts have also been presented (Carberry, 1962). Dynamic methods for determining macropore and micropore diffusivities in bidisperse catalysts have been discussed earlier (Hashimoto and Smith, 1974).

This note discusses the use of a single-pellet reactor for determining the diffusivities, effectiveness factor and the intrinsic rate constant for bidisperse catalysts and the error involved in the determination of the intrinsic rate constant if the bidisperse porous catalyst is approximated as monodisperse.

THEORETICAL ANALYSIS

It will be assumed that the reaction is isothermal, irreversible and first order, and the cylindrical pellet is made from spherical particles. The dimensionless conservation equations presented earlier for spherical pellets (Örs and Dõgu, 1979) modified for a cylindrical pellet exposed to the reactant on one plane surface are